MSDE

PAPER

View Article Online
View Journal | View Issue

Cite this: *Mol. Syst. Des. Eng.*, 2024, 9, 399

Mesoporous degradable chitosan-based monoliths: synthesis and applications toward water purification†

Jyoti Devi Katiyar and Subrata Chattopadhyay *

Received 11th November 2023,
Accepted 1st January 2024

DOI: 10.1039/d3me00180f

rsc.li/molecular-engineering

The sustainable synthesis of porous polymer monoliths has significant advantages over powdered porous polymers and is capable of adsorbing multiple types of pollutants efficiently from water. They are important as an easily affordable material for water purification. Herein, we report the synthesis of mesoporous chitosan, PEG monoliths, *via* the crosslinking of chitosan with PEG-diacrylate macro-crosslinkers using aza-Michael reactions in water. The surface area and pore volume are tuned by varying the crosslinking density and length of the macro-crosslinker. The materials show very good thermal and chemical stability against organic and aqueous (within pH 2–9) solvents. The monolith is capable of removing a wide range of both organic and inorganic pollutants, such as anionic dyes, metal ions, iodine, and pharmaceuticals, from contaminated water. The reusability of the monolith after it is regeneration by releasing the adsorbed pollutant is important for its affordable practical application. In addition, the monolith can be completely degraded in a strong alkaline solution to quantitatively recycle the chitosan derivative.

Design, System, Application

Recently, porous polymers have been regarded as one of the most efficient adsorbents for water treatment. With continuous sustainable development, the next generation of porous polymers is ideally (i) developed from sustainable resources, (ii) efficient in capturing a range of pollutants from water simultaneously, (iii) can be reused for multiple cycles, and (iv) remains disposable/degradable after its lifetime to inhibit additional plastic pollution. Herein, we report the preparation of a chitosan-based mesoporous polymer monolith, which is capable of efficiently removing multiple pollutants from water. Porosity can be tuned by controlling both the degree of crosslinking and the length of the PEG-based macro crosslinker used. Such monoliths can be efficiently reused for multiple cycles and degraded completely to recover the initial chitosan derivative.

1. Introduction

Due to rapid industrial developments in the last century, water pollution appears as a pressing global concern.[1–4] A recent report from the World Health Organization states that nearly three billion people are currently suffering from insufficient availability of safe drinking water.[5] Therefore, developing cost-effective materials and techniques for the sequestration of toxic contaminants from water has gained significant research priority in recent years.[6] Several strategies were developed and reported in the recent past to purify water, such as adsorption,[7,8] photodegradation,[9,10] electrochemical oxidation,[1] *etc.* Among these, adsorption has been regarded as one of the simplest, most efficient, and cost-effective ways for the separation of trace contaminants from water.[11]

Recently, different types of materials, such as microgels,[12] hydrogels,[13–15] aerogels,[16] metal–organic frameworks (MOF),[17–20] covalent organic frameworks (COF),[21,22] porous polymers[5,23,24] *etc.* were developed and used as adsorbents for water treatment. Among them, hydrogels and aerogels are largely macroporous.[25] Though in a few cases, the term, 'microporous hydrogel,' is used, it is likely to emphasise their micro-dimensional pores that are within the range of 4–40 μm.[26] MOF, COF, and porous polymers are generally advantageous for such applications due to their higher surface area and presence of micropores (with pore diameter of <2 nm) and mesopores (with pore diameters of 2–50 nm). Compared to MOF, porous polymers arguably have advantages, such as better thermal and chemical stability (due to the covalent polymeric network), the presence of various functional backbones, easy synthesis *etc.*, making them materials of choice in applications like water purification.

Department of Chemistry, Indian Institute of Technology Patna, Bihta, Patna 801106, Bihar, India. E-mail: sch@iitp.ac.in

† Electronic supplementary information (ESI) available. See DOI: https://doi.org/10.1039/d3me00180f

In recent years, several examples of functional porous polymers have been reported for water purification.[5,27] This includes typical porous polyamines,[28] polyaminoamides[29] and other ionic porous polymers,[30,31] porphyrin rings introduced into porous polymers,[32] β-cyclodextrin-based porous polymers,[33] *etc.* However, at some point, further developments are necessary. For example, (i) in the context of practical use and sustainable materials, it is desirable to build such materials from renewable/sustainable resources *via* easily affordable techniques.[34] There are few reports on these aspects to prepare lignin[35] and chitosan-based porous polymers,[36] and most of them are primarily macroporous—very few of them are actually microporous and mesoporous polymers.[37–40] (ii) In addition, most of the reported micro and mesoporous polymers are mostly powder-like materials, which lack further processability. Herein porous polymer monoliths are a better choice for applications like chromatography.[41,42] In the recent past, several radical-based approaches[43] reported porous polymer monoliths, but the majority of them were macroporous materials.[44,45] (iii) There are extremely few materials which are known to adsorb a range of pollutants under ambient conditions, which is an important quality from a practical viewpoint, and (iv) almost all reports focused on the reusability of the materials for multiple cycles of repeatable use. However, it is important to note that all reusable materials have a limited lifetime, beyond which it is desirable that the material should be degradable and recyclable to achieve the original starting materials or their derivatives. This will help avoid plastic pollution and contribute to a circular economy.

Herein, we report the design and synthesis of mesoporous chitosan-PEG monoliths, which can adsorb different types of pollutants simultaneously, and thus, they are a material of choice for water purification. Chitosan is an important class of natural polyamines,[46,47] and applications of chitosan-based adsorbents are well known in the context of environmental remediation.[48,49] However, very few chitosan-based microporous and mesoporous materials are reported in the literature. Two common approaches report the synthesis of microporous and mesoporous chitosan and involve (i) the use of a suitable template to attach chitosan onto it and (ii) phase separation. For example, Zhang *et al.* reported the fabrication of porous zeolites/chitosan monoliths[50] and Wang *et al.* prepared graphite oxide-doped porous chitosan monoliths.[51] However, in both cases, the surface area and pore volume were not reported accurately. Very recently, Hajili *et al.* reported a hierarchically porous chitosan monolith fabricated *via* a thermally induced phase separation approach, resulting in a porous structure with a total surface area of 144 $m^2\ g^{-1}$.[52] In the recent past, the use of suitable crosslinkers and changing the crosslinking density has evolved as an established mechanism to develop porous polymers, but such a process has never been well explored in the context of chitosan. Here, we use PEG diacrylate as a macro crosslinker, which is hydrophilic and soluble in water, thereby allowing us to prepare materials with wide-ranging crosslinking densities. Chitosan is soluble effectively only in slightly acidic water, and therefore, hydrophobic crosslinkers are not suitable for such an approach. It is expected that the presence of both amines and ether functionalities, such as combinations of π-electron-rich esters linkages, will facilitate the efficient adsorption of a wider variety of pollutants.[53] Initially, surface area and pore volume are tuned *via* the structure–porosity relationship of a series of monoliths by varying the crosslinking density and length of the macro-crosslinker. Next, the application of the product is demonstrated to capture a range of pollutants efficiently. While the monoliths show significant stability under ambient pH, they can be easily degraded under strongly alkaline conditions, and the original chitosan derivative can be recovered quantitatively.

2. Results and discussions

2.1. Synthesis and characterization of porous chitosan-PEG monoliths

In the current work, porous chitosan monoliths are prepared *via* crosslinking of chitosan (calculated degree of deacetylation ~75%, Fig. S1†) with PEG-diacrylate *via* aza-Michael addition reaction in the presence of $NaHCO_3$ as a base in water (Scheme 1). In this approach, hydrophilic oligomeric PEG-diacrylate was used as a macro-crosslinker and soft template to generate a porous network. A slight difference in diffusion coefficient (Fig. S2†) between chitosan and PEG-diacrylate is expected to contribute to the nucleation/spinodal decomposition, helping generate a porous morphology.[54] In general, during such a crosslinking process, the degree of polymerization/molecular weight continuously increases with time, which results in more asymmetric spinodal decomposition.[55] Such phase separation generates higher porosity until an optimum crosslinking is achieved (solvent during such phase separation acts as porogen). Crosslinking between chitosan and PEG-diacrylate in water ($NaHCO_3$ as a base) leads to the formation of a gel. The $NaHCO_3$ is removed from the gel by immersing the gel in excess water for 24 hours. Thereafter, the gel is dried using a freeze-dryer to obtain the purified monolith. The removal of $NaHCO_3$ is confirmed by analyzing the elemental composition using the EDX analysis technique (Fig. S3†). To further tune the surface area and porosity, different molecular weights of PEG segments are used with varying degrees of crosslinking (Table S1†). This effort resulted in the preparation of six different porous polymer monoliths with varying surface areas and pore volumes, but with comparable molecular backbones (Scheme 1).

After synthesis, the monoliths were characterized *via* solid-state ^{13}C and IR spectroscopy. In ^{13}C NMR spectra (Fig. 1a), characteristic alkene peaks (C=C) of acrylate found at ~130 ppm disappeared in the monolith. Other characteristic peaks of chitosan and PEG backbone could be observed clearly. In the IR spectra (Fig. 1b and S4†), the characteristic band of sp^2 CH stretching frequency at 2880

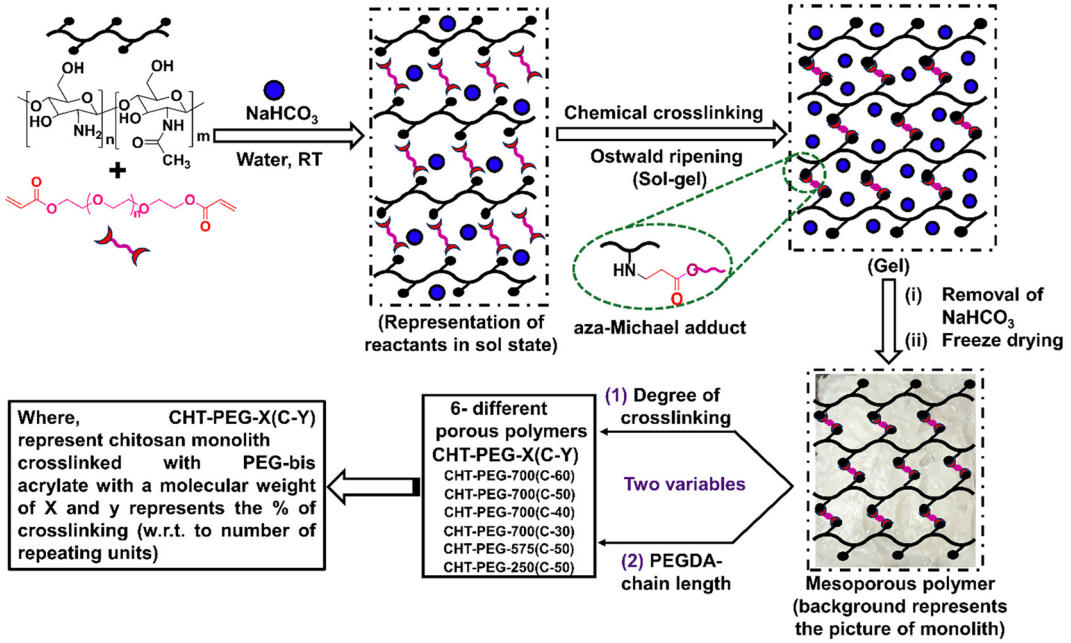

Scheme 1 Synthesis of porous chitosan-PEG monoliths.

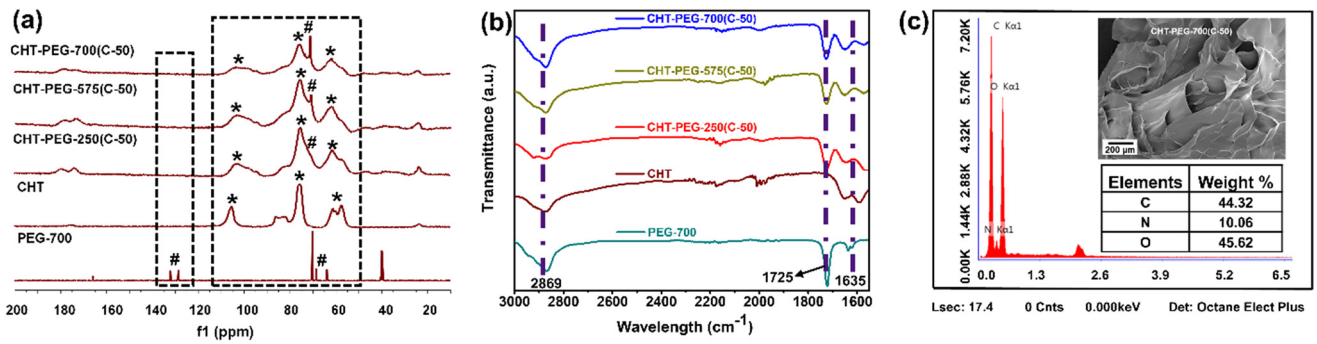

Fig. 1 Molecular characterization of porous chitosan-PEG monoliths *via* (a) solid-state ^{13}C NMR spectral analysis, (b) IR spectral analysis, and (c) EDX analysis (inset: SEM image corresponding to the EDX analysis).

cm^{-1} disappeared in the IR spectra of the monolith. However, the presence of a weak band in a similar region is characteristic of sp^3 CH_2 methylene peaks of chitosan. In addition, the characteristic band of the ester group (~1725 cm^{-1}) of PEG diacrylate clearly appeared in the monolith. This confirms the formation of monoliths *via* the aza-Michael reaction between chitosan and PEG diacrylate. Moreover, EDX analysis (Fig. 1c) confirmed the presence of C, N, and O as main elements. In addition, powder XRD analysis revealed the amorphous nature of the monoliths (Fig. S5†).

To tune the surface area and pore volume of the monoliths, different samples were prepared by varying two parameters: (i) PEG crosslinkers with different molecular weights and (ii) changing the degree of crosslinking. The surface area of the monoliths was analyzed using a low-temperature nitrogen adsorption–desorption isotherm (BET analysis at 77 K). BET analysis of different crosslinked monoliths [CHT-PEG-700(C-30), CHT-PEG-700(C-40), CHT-PEG-700(C-50), and CHT-PEG-700(C-60)] clearly signified that surface area and porosity increases with an increase in the degree of crosslinking till 50%, but it decreases thereafter (Fig. 2a). In addition, PEG diacrylate with different molecular weights (PEG-250, PEG-575, and PEG-700) were used as crosslinkers to confirm that highest surface area was noted when PEG-700 was used (Fig. 2b). Additionally, NLDFT (Fig. 2c and d) and BJH analysis (Table 1) also supported the same and confirmed that the monoliths are predominantly mesoporous with an average pore size of 2.7–3.2 nm. Through all the analysis and structure–property correlation, it can be concluded that CHT-PEG-700(C-50) possesses the highest surface area of 172 m^2 g^{-1} and total pore volume of 0.229 cc g^{-1}. The details of the analyses for all materials are tabulated in Table 1.

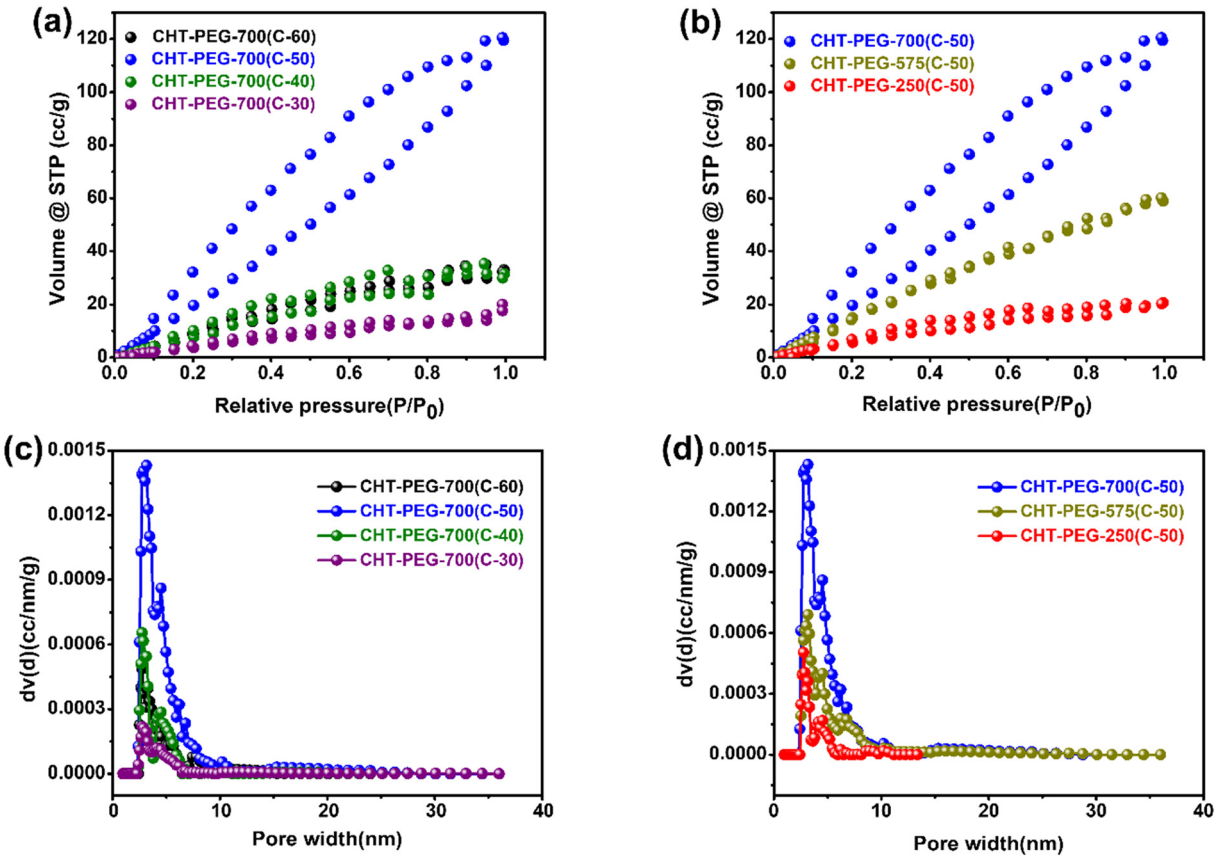

Fig. 2 Porosity and surface area analysis of the chitosan-PEG monoliths, nitrogen adsorption–desorption isotherms at 77 K at (a) different crosslinked densities of PEG-700 and (b) different molecular weights of the PEG crosslinker. The pore size distribution of the chitosan-PEG monoliths was determined by the NLDFT method with (c) different crosslinked densities using PEG-700 and (d) different molecular weights of the PEG crosslinker.

Table 1 Porosity and surface area analysis of chitosan-PEG monoliths

		DFT method		BJH method	
Porous polymer monolith	Surface area ($m^2\ g^{-1}$)	Pore size (nm)	Pore volume (cc g^{-1})	Pore size (nm)	Pore volume (cc g^{-1})
CHT-PEG-700(C-30)	30.375	2.769	0.024	2.82	0.027
CHT-PEG-700(C-40)	78.09	2.769	0.051	1.918	0.066
CHT-PEG-700(C-50)	172.0	3.169	0.229	1.92	0.071
CHT-PEG-700(C-60)	72.825	2.769	0.051	1.713	0.045
CHT-PEG-575(C-50)	123.84	3.169	0.135	1.92	0.078
CHT-PEG-250(C-50)	39.18	2.77	0.029	2.45	0.025

Furthermore, the porous morphology of the polymers was visualized by FESEM analysis (Fig. 3 and S6† for overview images). The micrographs support the formation of mesopores and depict characteristic pores formed by spinodal decomposition (solvent acts as a porogen and is removed by freeze-drying).

The thermal stability of the porous polymer was analyzed *via* thermogravimetric analysis, confirming that the monolith is thermally stable till 200 °C ($T_{d,10}$) (Fig. S7a†). A small weight loss (~5%, due to the release of residual water) at ~100 °C was unavoidable due to the hygroscopic nature of the monolith backbone. It is important to note that the thermal stability of the monolith is slightly lower than the original chitosan polymer, which can be ascribed to the thermal degradation of the PEG macro-crosslinker at ~200 °C.[56,57] Additionally, the chemical stability of the monolith in various solvents was determined *via* gravimetric analysis (Fig. S7b†). Gravimetric analysis indicates that there is no significant weight loss upon exposure for 24 hours to various solvents, such as $CHCl_3$, DMSO, THF, MeOH, DMF, water, acidic water (pH ~0.1), and slightly alkaline water (till pH ~9). Additionally, IR analysis of post-treated material affirms that the molecular structure remains intact (Fig. S8†). These observations support excellent thermal and chemical stability of the monolith for different applications.

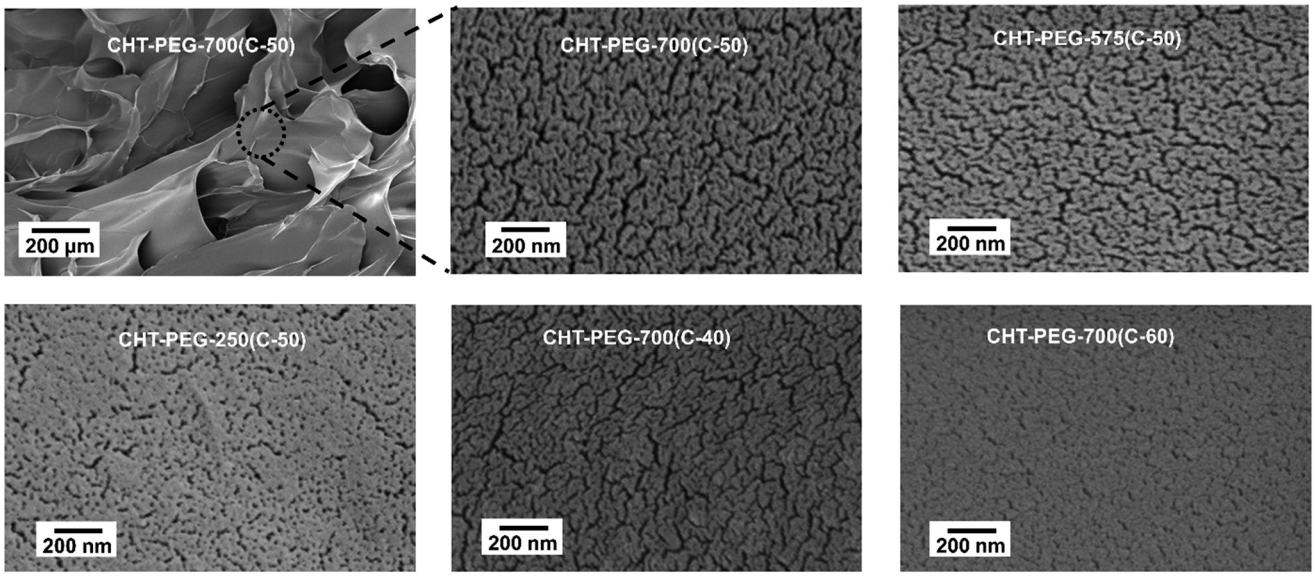

Fig. 3 FESEM micrographs of the chitosan-PEG monoliths.

2.2. Application of the monolith for water purification

This section of the study narrates the adsorption capacity of the monolith toward different pollutants and thereby its applicability for water purification. As per literature, varieties of pollutants have been identified to be present in water, such as organic dyes, iodine, metal ions, and pharmaceuticals. To study the adsorption capacity of the monoliths for different types of pollutants, we selected a range of well-known pollutants from different subtypes. For example, Congo red (CR) and methyl orange (MO) were chosen as model organic dyes, lead (Pb(II)) and copper (Cu(II)) as metal ions, ibuprofen as a model pharmaceutical compound, and iodine was chosen as an important example of nuclear waste. A systematic study of CR, MO and iodine adsorption isotherms using all six porous monoliths (as prepared earlier) clearly indicates that adsorption capacity enhances with increasing surface area and CHT-PEG-700(C-50) appeared to be the best material in terms of adsorption capacity (Fig. S9–S11 and Tables S2–S4†). Therefore CHT-PEG-700(C-50) was further explored in detail to

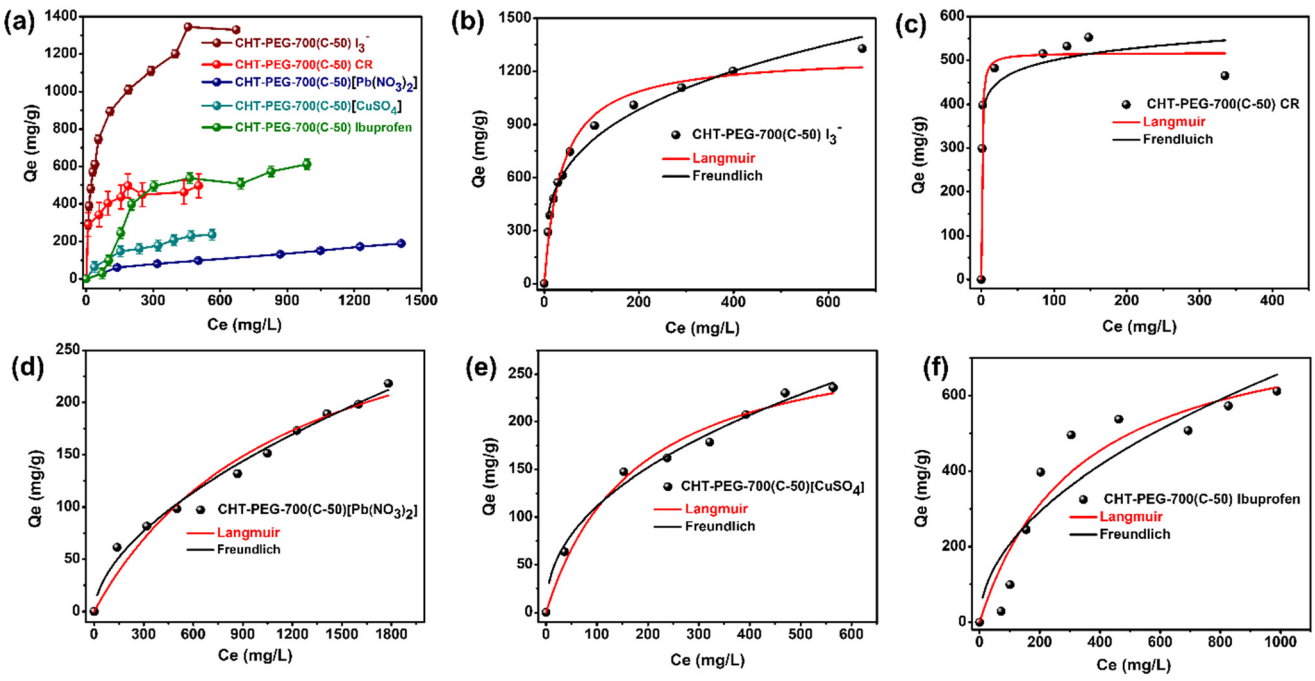

Fig. 4 (a) Pollutant adsorption of CHT-PEG-700(C-50) in water, Langmuir and Freundlich adsorption isotherm models for (b) I_3^- (c) CR, (d) [$Pb(NO_3)_2$], (e) $CuSO_4$, and (f) ibuprofen removal by the adsorbent, CHT-PEG-700(C-50).

understand its efficiency in removing all the different pollutants mentioned earlier to purify water.

To study that, we first investigated the individual adsorption isotherms of different pollutants using CHT-PEG-700(C-50) (Fig. 4). To study the adsorption isotherm, aqueous solutions of different pollutants with a range of concentrations were prepared separately, and the monolith was immersed in each solution for 24 hours. After reaching the equilibrium, the solutions were analyzed using UV-vis spectroscopy. Furthermore, Langmuir and Freundlich isotherm models were used to fit and calculate the adsorption capacity of CHT-PEG-700(C-50) for different pollutants. The results are summarized in Table 2. The results indicate that all the adsorption isotherms fitted better with the Langmuir model with improved R^2 values (0.90–0.98). The theoretical adsorption capacity values closely matched the experimental values using the Langmuir model. The calculated adsorption capacity of CHT-PEG-700(C-50) for I_3^-, CR, Pb(II), Cu(II), and Ibuprofen were 1290.0, 517, 345, 302, and 832 mg g^{-1}, respectively. To compare the adsorption capacity observed here with that of the state-of-the-art adsorbents, we compared the current monoliths with previously reported chitosan-based adsorbents (Table S5†). The results indicate that the current monolith has superior adsorption capacity compared to most other chitosan-based adsorbents with the added advantage that it is capable to remove multiple pollutants alone.

In the next step, adsorption kinetics for all the individual pollutants in water were studied using UV-vis spectroscopy. The kinetic plots for all the pollutants are shown in Fig. 5. The data clearly represents faster adsorption kinetics for iodine and CR. In both cases, more than 90% of the pollutants were removed within an hour. However, kinetics were much slower for metal ions and ibuprofen. For all these cases, nearly 3 to 8 hours were required to remove the

Table 2 Adsorption isotherm parameters of the Langmuir and Freundlich model for I_3^-, CR, $[Pb(NO_3)_2]$, $CuSO_4$, and ibuprofen removal using CHT-PEG-700(C-50)

		Langmuir model			Freundlich model		
Adsorbent	Adsorbate	Q_m (mg g^{-1})	K_L (L mg^{-1})	R^2	K_F (L mg^{-1})	n	R^2
CHT-PEG-700(C-50)	I_3^-	1290.62	0.026	0.98	214.09	3.47	0.97
CHT-PEG-700(C-50)	CR	517.38	1.32	0.96	359.38	13.87	0.58
CHT-PEG-700(C-50)	$[Pb(NO_3)_2]$	344.59	0.001	0.97	2.98	1.75	0.98
CHT-PEG-700(C-50)	$CuSO_4$	302.36	0.0056	0.98	14.23	2.23	0.97
CHT-PEG-700(C-50)	Ibuprofen	831.69	0.003	0.90	20.23	1.98	0.77

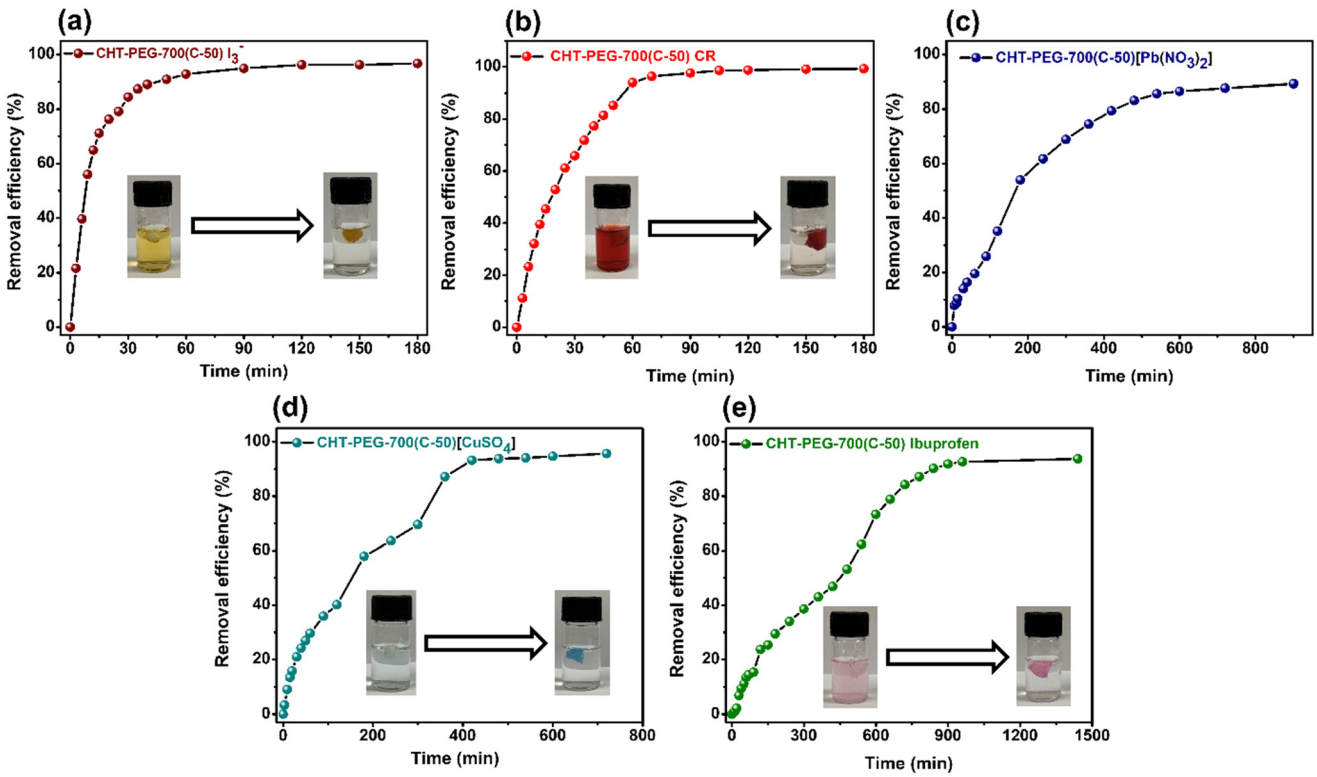

Fig. 5 Pollutant adsorption kinetics of (a) I_3^- (b) CR, (c) $[Pb(NO_3)_2]$, (d) $CuSO_4$, and (e) ibuprofen removal by the adsorbent, CHT-PEG-700(C-50).

respective adsorbates. Although these kinetics are slower, the speed of activity is still comparable with other reports in the context of metal ions (Pb(II), and Cu(II)) and pharmaceuticals under ambient conditions (in several cases, slightly faster kinetics was noted at acidic pH, which is similar to our observations at pH ~5 as detailed in Fig. S13,† but this is not very relevant in the context of practical applications because pH of usable water is generally ~7, Tables S6 and S7†). In addition, slow adsorption results in a multistep process, as revealed in Fig. 5c–e—probably due to the unavoidable influence of other ions and the presence of a heterogeneous functional surface (a range of different functional moieties). Furthermore, the adsorption kinetics were studied using pseudo-first order and pseudo-second order kinetic models (Fig. S12†), and the results are summarized in Table S8.† Better correlation coefficients (R^2) revealed that the kinetics followed the pseudo-second-order model.

The reusability of the chitosan-PEG monolith is important for sustainable and affordable day-to-day application in the current context. To check the reusability, the (CR, iodine, metal ions, and ibuprofen) chitosan porous monolith loaded with pollutants was first treated with a suitable solvent to remove the adsorbed pollutants completely and subsequently reused for consecutive adsorption cycles (Fig. S14†). The re-release of the adsorbed pollutants was monitored *via* UV-vis spectroscopy, and their complete removal from the monolith matrix was confirmed *via* EDX mapping (Fig. S15 and S16†). The process was repeated for at least four consecutive cycles revealing excellent reusability of the materials for multiple cycles of adsorption.

2.3. Efficacy to adsorb a mixture of pollutants simultaneously

For a practical application for the purification of water, it is important to note that polluted water contains a mixture of different impurities. It is very important that the monolith fabricated here should be equally useful to simultaneously adsorb and purify a mixture of pollutants in water. Therefore, the current material is tested to purify a mixture of pollutants at the same time (Fig. 6). For that, an aqueous solution containing a mixture of pollutants, such as CR, iodine, ibuprofen, and metal ions (Pb^{2+}), was prepared. The monolith was immersed in that solution, and after some time of equilibration, the concentration of the solution was measured using UV-vis spectroscopy. The disappearance of all the relevant peaks at ~346 and 498 nm (for CR), 288 nm and 354 nm (for I_3^-), 205 nm (Pb^{2+}), and 220 nm (for ibuprofen) revealed that the monolith can remove pollutants simultaneously from a mixture. Additionally, a reusability study with a mixture of pollutants clearly affirmed that the current monolith is reusable for at least four consecutive cycles (Fig. 6c).

2.4. Degradation studies

While talking about adsorbents, we are generally concerned with their reusability (in some manuscripts, this is also described as recyclability). However, it is important to note that every material has its own lifetime (in the context of desorption and reuse) and only can be reused for a limited number of cycles. Therefore, the degradation of polymeric materials should be an important concern for practical and industrial use – otherwise, non-degradable polymers will contribute to plastic pollution after their overall lifetime of use, which is already a serious global concern. In this regard, chitosan and other degradable polymer-based monoliths can play a vital role. The current monolith is composed of chitosan and a PEG backbone, which are expected to degrade under alkaline conditions (a known condition for the degradation of the PEG backbone) and in the presence of lysozyme (a known condition for the degradation of chitosan backbone). In contrast, the monolith was also treated in ambient water (pH ~7) to affirm its stability within the testing period (served as a control).

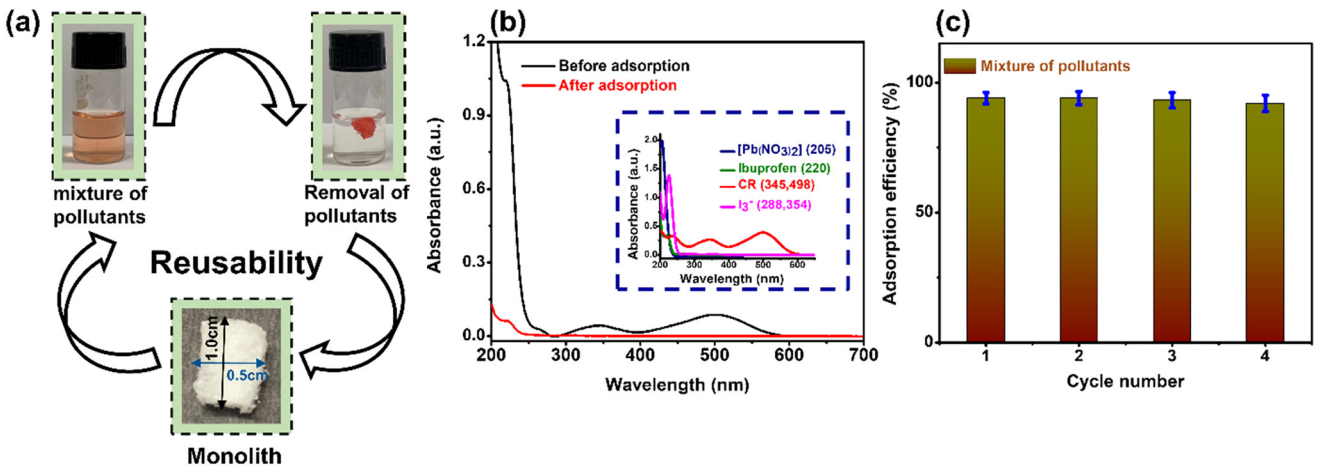

Fig. 6 Adsorption and reuse of the monolith to capture a mixture of pollutants simultaneously, (a) an original image of chitosan monoliths used for adsorption and reuse, (b) UV-vis spectra of polluted water containing a mixture of pollutants before and after adsorption, and (c) reusability for four consecutive cycles of capturing pollutants.

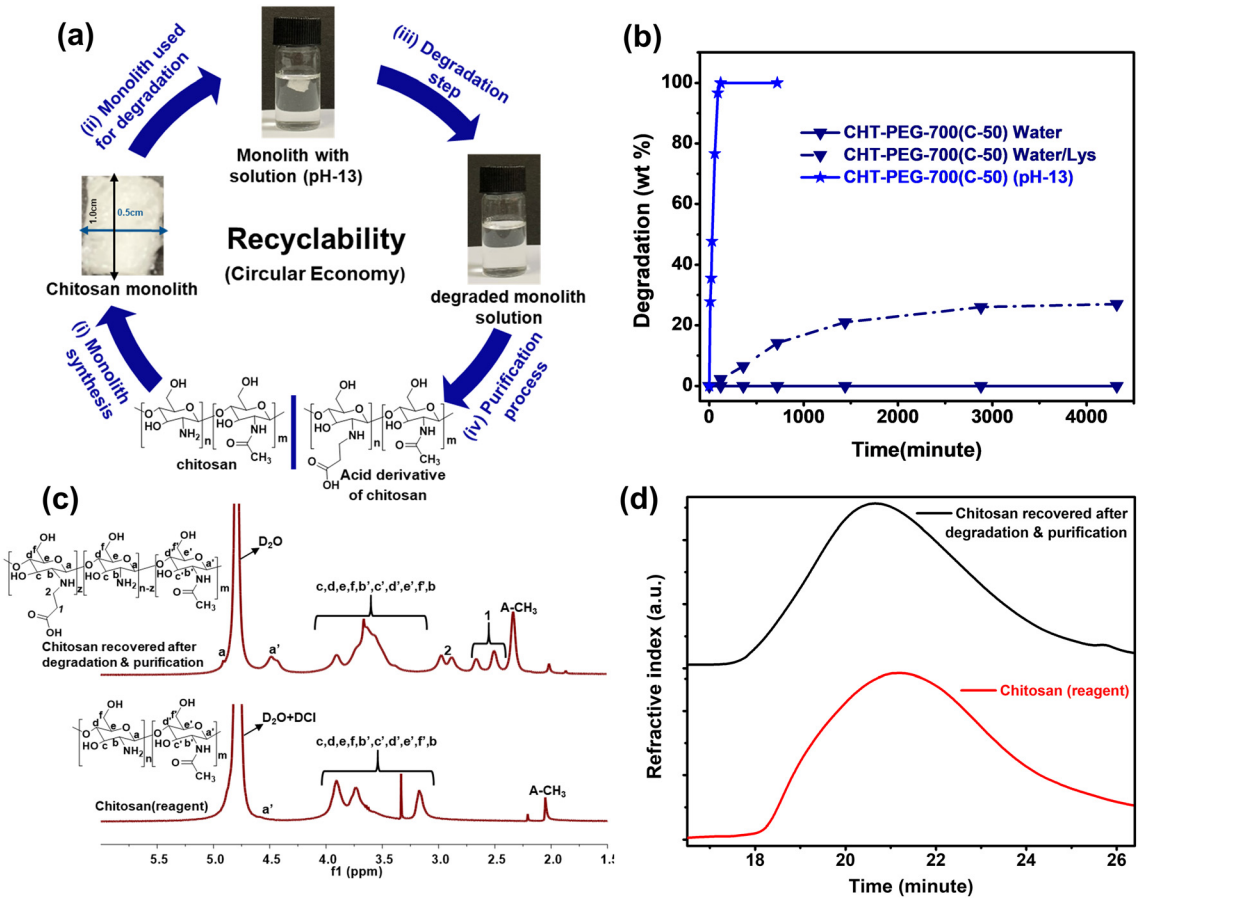

Fig. 7 (a) Schematic representation of the synthesis, degradation of the chitosan monolith in various steps (i–iv), (b) degradation kinetics under different conditions *via* the gravimetric method, (c) NMR spectra, and (d) SEC chromatogram of recovered chitosan derivatives after the degradation of the monolith.

As discussed, the kinetics of degradation were studied *via* the gravimetric method under three conditions: (i) alkaline water (0.1 M NaOH solution, pH > 13), (ii) aqueous lysozyme solution (concentration = 0.3 mg mL^{-1}), and (iii) distilled water (pH ~6.8). The monolith was immersed fully in a given solution for three days, and degradation was monitored gravimetrically (Fig. 7b). The data clearly signifies that the monolith degraded very fast under alkaline conditions with complete degradation within 2 hours/120 minutes, while a slower degradation rate was observed (~30% in 72 hours) in the lysozyme solution. Importantly, no change was noted in pure water, again affirming that material can be used for water purification under ambient conditions.

Complete degradation was noted *via* the gravimetric method under alkaline conditions, therefore, the degraded monolith solution was further characterized to understand the nature of degraded products and assess their recovery. From existing knowledge, one can expect that under such conditions, the ester linkage and PEG backbone will degrade preferentially at a faster rate. To gain further insight, the ^{1}H NMR spectra of the degraded monolith were analyzed (Fig. S17a†). The characteristic peak revealed the presence of both PEG and chitosan segments in the degraded product. The degraded solution was precipitated in acetone to separate the chitosan and PEG segments. The precipitated polymer was collected and characterized *via* ^{1}H NMR (Fig. 7c), IR (Fig. S17b†) and SEC (Fig. 7d) analyses. The analyses clearly revealed that the precipitated polymer contained the chitosan fragment, while both IR spectra revealed the presence of the acid group. Furthermore, the SEC analysis revealed that the molecular weight of the fragmented chitosan (recovered after degradation) is exactly the same as the molecular weight of the starting material (chitosan), which supported the proposed mechanism (Fig. S18†) of the degradation of the monolith within the given time frame (2 hours). Controlled analysis further confirmed that this method leads to quantitative (~95–100%) regeneration of chitosan derivative which is equivalent to the amount of chitosan used to synthesize the monolith.

3. Conclusions

We have developed a sustainable strategy to synthesize mesoporous chitosan-PEG monolith in water using $NaHCO_3$ as a base under ambient conditions. The study of structure and porosity using a library of monoliths revealed that the highest surface area could be achieved when PEG-700 was used as a macro-crosslinker with 50% crosslinking density.

The materials fabricated here showed very good thermal and chemical stability. The monolith was efficient in removing a wide range of pollutants (such as Pb^{2+}, Cu^{2+}, Congo red, iodine, and ibuprofen) from water simultaneously and could be reused for at least four consecutive cycles. In addition, due to the presence of degradable backbones, the monolith could be easily degraded in strong alkaline solutions—which when done in a controlled way leads to the regeneration of starting chitosan polymer derivative in a quantitative way. Therefore, this report demonstrates one of the first examples of preparing porous polymer monolithic adsorbents for efficient water purification for multiple cycles. At the end of its lifetime, the monolith can be degraded back to generate the derivatives of its starting materials quantitatively, which certainly adds to the circular economy concept.

Associated content

All experimental details, additional analytical data and figures are given in the ESI.†

Data availability

All additional data supporting this research work is included in the ESI.†

Author contributions

All experiments and analyses were performed by Jyoti Devi Katiyar. Subrata Chattopadhyay conceptualized and supervised the work. The manuscript was written through the contributions of all authors. All authors approve the final version of the manuscript.

Conflicts of interest

The authors declare no competing financial interests.

Acknowledgements

The authors thank the Indian Institute of Technology Patna (IITP) for generous financial and infrastructural support. JDK thanks IITP for the Research Fellowship. SC gratefully acknowledges CSIR grant-in-aid, scheme No. 02(0370)/19/EMR-II, for financial support. All authors would like to gratefully acknowledge SAIF and IITP for NMR analysis.

References

1 X. Zhu and D. Jassby, *Acc. Chem. Res.*, 2019, **52**, 1177–1186.
2 P. J. J. Alvarez, C. K. Chan, M. Elimelech, N. J. Halas and D. Villagrán, *Nat. Nanotechnol.*, 2018, **13**, 634–641.
3 S. J. Tesh and T. B. Scott, *Adv. Mater.*, 2014, **26**, 6056–6068.
4 M. Avais and S. Chattopadhyay, *J. Mater. Chem. A*, 2022, **10**, 20090–20100.
5 Q. Sun, B. Aguila, Y. Song and S. Ma, *Acc. Chem. Res.*, 2020, **53**, 812–821.
6 K. Bakker, *Science*, 2012, **337**, 914–915.
7 S. Kumari, M. Avais, J. D. Katiyar, Y. K. Suman and S. Chattopadhyay, *J. Polym. Res.*, 2022, **29**, 293.
8 Y. Song, J. Phipps, C. Zhu and S. Ma, *Angew. Chem.*, 2023, **62**, e202216724.
9 S. Gharbi, N. Méndez-Gil, K. Hriz, M. Majdoub and B. Gómez-Lor, *ACS Appl. Polym. Mater.*, 2023, **5**, 2359–2366.
10 E. Elias, C. Sarathchandran, S. Joseph, A. K. Zachariah, J. Thomas, D. Devadasan, F. G. Souza Jr and S. Thomas, *J. Appl. Polym. Sci.*, 2021, **138**, 50612.
11 I. Ali, *Chem. Rev.*, 2012, **112**, 5073–5091.
12 S. Kumari, M. Avais and S. Chattopadhyay, *ACS Appl. Polym. Mater.*, 2023, **5**, 1626–1645.
13 C. B. Godiya, L. A. Martins Ruotolo and W. Cai, *J. Mater. Chem. A*, 2020, **8**, 21585–21612.
14 K. Ravishankar and R. Dhamodharan, *React. Funct. Polym.*, 2020, **149**, 104517.
15 M. Avais and S. Chattopadhyay, *Polymer*, 2019, **180**, 121701.
16 Y. Fu and Z. Guo, *J. Mater. Chem. A*, 2022, **10**, 8129–8158.
17 A. V. Desai, B. Manna, A. Karmakar, A. Sahu and S. K. Ghosh, *Angew. Chem., Int. Ed.*, 2016, **55**, 7811–7815.
18 B. Van de Voorde, B. Bueken, J. Denayer and D. De Vos, *Chem. Soc. Rev.*, 2014, **43**, 5766–5788.
19 C. Wang, J. Kim, J. Tang, J. Na, Y.-M. Kang, M. Kim, H. Lim, Y. Bando, J. Li and Y. Yamauchi, *Angew. Chem., Int. Ed.*, 2020, **59**, 2066–2070.
20 Z. Zhang, C. Wang, Y. Yao, H. Zhang, J. Na, Y. Zhou, Z. Zhu, J. Qi, M. Eguchi, Y. Yamauchi and J. Li, *Chem. Sci.*, 2022, **13**, 9159–9164.
21 A. K. Mohammed and D. Shetty, *Environ. Sci.: Water Res. Technol.*, 2021, **7**, 1895–1927.
22 Z. Xia, Y. Zhao and S. B. Darling, *Adv. Mater. Interfaces*, 2021, **8**, 2001507.
23 L. Tian, S. Zhou, J. Zhao, Q. Xu, N. Li, D. Chen, H. Li, J. He and J. Lu, *J. Hazard. Mater.*, 2023, **441**, 129873.
24 S. Shingdilwar, S. Dolui, D. Kumar and S. Banerjee, *Mater. Adv.*, 2022, **3**, 665–671.
25 E. Sangeetha, R. Sharma, A. Narayanan, S. Varadaraj and R. Dhamodharan, *ACS Appl. Polym. Mater.*, 2022, **4**, 1764–1774.
26 Y. Chen, L. Huang, X. Dai, Q. Tian, M. Yu, M. Agheb, H. N. Chan, E. Poon, Z. Guo, K. R. Boheler and H. Wu, *J. Mater. Chem. B*, 2017, **5**, 9291–9299.
27 P. Zhang, M. He, W. Teng, F. Li, X. Qiu, K. Li and H. Wang, *Green Energy Environ.*, 2023, DOI: **10.1016/j.gee.2023.11.001**.
28 S. Peter, N. Lyczko, D. Gopakumar, H. J. Maria, A. Nzihou and S. Thomas, *Waste Biomass Valoriz.*, 2021, **12**, 4777–4804.
29 M. Avais and S. Chattopadhyay, *ACS Appl. Polym. Mater.*, 2021, **3**, 789–800.
30 G. Xiong, B.-B. Wang, L.-X. You, B.-Y. Ren, Y.-K. He, F. Ding, I. Dragutan, V. Dragutan and Y.-G. Sun, *J. Mater. Chem. A*, 2019, **7**, 393–404.
31 D. Xu, J. Guo and F. Yan, *Prog. Polym. Sci.*, 2018, **79**, 121–143.
32 Y. Wang, X. Cui, P. Zhang, Y. Wang and W. Lu, *Environ. Technol. Innovation*, 2023, **29**, 102972.

33 L. Sun, G. Xu, Y. Tu, W. Zhang, X. Hu, P. Yang, D. Wu, Y. Liang, D. Wei, A. Li and X. Xie, *Water Res.*, 2022, **222**, 118917.
34 M. Sevilla, N. Díez and A. B. Fuertes, *ChemSusChem*, 2021, **14**, 94–117.
35 M. Yao, X. Bi, Z. Wang, P. Yu, A. Dufresne and C. Jiang, *Int. J. Biol. Macromol.*, 2022, **223**, 980–1014.
36 J. Wang and S. Zhuang, *J. Cleaner Prod.*, 2022, **355**, 131825.
37 L. Szabó, X. Xu, K. Uto, J. Henzie, Y. Yamauchi, I. Ichinose and M. Ebara, *ACS Appl. Mater. Interfaces*, 2022, **14**, 4004–4021.
38 X. Ge, Y. Ma, X. Song, G. Wang, H. Zhang, Y. Zhang and H. Zhao, *ACS Appl. Mater. Interfaces*, 2017, **9**, 13480–13490.
39 M. Sakai, H. Hori, T. Matsumoto and M. Matsukata, *ACS Appl. Mater. Interfaces*, 2023, **15**, 22395–22402.
40 A. Primo, A. Forneli, A. Corma and H. García, *ChemSusChem*, 2012, **5**, 2207–2214.
41 D. Kim, H. J. Kim, H. Kim and J. Y. Chang, *ACS Appl. Polym. Mater.*, 2021, **3**, 1385–1394.
42 M. Avais, S. Kumari and S. Chattopadhyay, *Soft Matter*, 2021, **17**, 6383–6393.
43 S. A. Saba, M. P. S. Mousavi, P. Bühlmann and M. A. Hillmyer, *J. Am. Chem. Soc.*, 2015, **137**, 8896–8899.
44 I. Nischang and T. J. Causon, *TrAC, Trends Anal. Chem.*, 2016, **75**, 108–117.
45 F. Svec, *J. Chromatogr. A*, 2010, **1217**, 902–924.
46 V. Zargar, M. Asghari and A. Dashti, *ChemBioEng Rev.*, 2015, **2**, 204–226.
47 J. D. Katiyar and S. Chattopadhyay, *Carbohydr. Polym.*, 2022, **287**, 119324.
48 E. Guibal, *Sep. Purif. Technol.*, 2004, **38**, 43–74.
49 J. Zhao, H. Liu, P. Xue, Y. Qi, Z. Lv, R. Wang, Y. Wang and S. Sun, *J. Hazard. Mater.*, 2023, **460**, 132435.
50 Y. Zhang, W. Yan, Z. Sun, C. Pan, X. Mi, G. Zhao and J. Gao, *Carbohydr. Polym.*, 2015, **117**, 657–665.
51 Y. Wang, X. Liu, H. Wang, G. Xia, W. Huang and R. Song, *J. Colloid Interface Sci.*, 2014, **416**, 243–251.
52 E. Hajili, A. Sugawara, T.-A. Asoh and H. Uyama, *ACS Sustainable Chem. Eng.*, 2023, **11**, 5473–5484.
53 T. Nabeshima, T. Inaba, N. Furukawa, T. Hosoya and Y. Yano, *Inorg. Chem.*, 1993, **32**, 1407–1416.
54 F. Wang, P. Altschuh, L. Ratke, H. Zhang, M. Selzer and B. Nestler, *Adv. Mater.*, 2019, **31**, 1806733.
55 G. Zhang, T. Yang, S. Yang and Y. Wang, *Phys. Rev. E*, 2017, **96**, 032501.
56 M. Avais and S. Chattopadhyay, *Macromol. Chem. Phys.*, 2022, **223**, 2200109.
57 J. D. Katiyar, A. Halder, M. Avais, H. Aidasani, O. Mukherjee and S. Chattopadhyay, *ACS Appl. Polym. Mater.*, 2023, **5**, 9742–9750.